doi:10.2489/jswc.2020.00086

Evolution of rock cover, surface roughness, and flow velocity on stony soil under simulated rainfall

L. Li, M.A. Nearing, V.O. Polyakov, M.H. Nichols, and M.L. Cavanaugh

Abstract: Erosion pavements occur commonly in many semiarid watersheds due to selective erosion. However, quantitative information regarding the dynamic feedback between soil erosion, surface morphology, and flow hydraulics as erosion pavement develops is limited. In order to quantify the spatiotemporal evolution of rock cover and surface roughness, and measure their effects on flow velocities as erosion pavement develops, a series of rainfall simulations were conducted on a 2 by 6.1 m soil plot under three slope treatments (5%, 12%, and 20%) with surface elevation and rock cover measurements. The total applied rainfall volume for each experimental replication ranging from 1,400 to 2,240 mm caused the development of erosion pavement. The results showed (1) rock cover increased from 15% to 90% as rainfall progressed, and the terminal rock cover was not slope gradient dependent; (2) random roughness was positively correlated with rock cover in the upper and middle plot sections, and increasing surface roughness and rock cover reduced the flow velocity following power functions; (3) surface roughness in the lower sections did not uniformly increase with increasing rock cover due to the formation of rills; (4) the terminal surface roughness values of full plots were 5.3 and 5.1 mm, 4.2 and 4.5 mm, and 2.9 and 3.2 mm for replications of 20%, 12%, and 5% slopes, respectively, indicating that steeper slopes produced greater surface roughness; (5) flow velocities measured at the end of experiments reached a relative constant value that was a function of unit flow rates alone for a given section; (6) hydraulic resistances were correlated with flow discharge, slope gradient, and rock cover, exhibiting no unique hydraulic coefficient for a given surface condition. These results improve our understanding of the evolution of semiarid hillslopes.

Key words: erosion pavement—flow hydraulics—slope-velocity-equilibrium—soil erosion

One of the major subjects in hydrology is understanding and quantifying the processes that control hydrological storages and fluxes at local, regional, and global scales (Moran et al. 1994). Erosion pavement is one result of hillslope evolution on semiarid watershed hillslopes (Nearing et al. 2017), which is defined by Shaw (1929) as the preferential erosion process in which finer materials are selectively washed out, armoring the surface with coarser materials, e.g., rocks. Abundant rock fragments are reported on the soil surface or in the soil profile on many semiarid hillslopes, including United States (Simanton and Toy 1994; Simanton et al. 1994; Polyakov et al. 2018a), Spain (Van Wesemael et al. 1996; Poesen et al. 1998) and China (Xia et al. 2018). The accumulation of rock fragments as erosion pavement develops are erosion-induced products and are known to be of paramount importance to the hydrological and erosion processes in semiarid landscapes where vegetation cover is relatively low (Nearing et al. 2005). A dynamic feedback between erosion, surface morphology and flow hydraulics is expected. Many research studies have been conducted to study the effects of rock cover on erosion processes (Abrahams et al. 1986; Parsons et al. 1990; Poesen et al. 1994; Poesen and Lavee 1994; Rieke-Zapp et al. 2007; Xia et al. 2018), while fewer have investigated how surface morphology evolves in response to erosion through the formation of erosion pavement and how the evolved surface morphology, in turn, affects flow hydraulics and erosion patterns. This lack of information is due in part to the difficulty of conducting the fieldwork for addressing these questions (Pelletier 2003).

Increasing trends of rock cover over time under simulated rainfall have been indicated in some studies (Rieke-Zapp et al. 2007; Xia et al. 2018; Lv et al. 2019); however, the spatiotemporal evolution of rock cover was not the emphasis in those studies. Generally, steeper slopes are associated with greater erosion potential, which is anticipated to result in a greater rock fragment exposure (cover percentage) along the hillslope profile. A positive relationship between rock cover and slope gradient has been reported in many semiarid environments. For example, a survey of the spatial distribution of surface rock along catenas in semiarid Arizona and Nevada was conducted by Simanton et al. (1994), and they found a logarithmic relationship between rock fragment cover and slope gradient, with greater rock cover associated with steeper parts of the hillslopes. Similar findings were also reported by Simanton and Toy (1994) and Poesen et al. (1998).

Accumulated rock fragments in stony soils tend to enhance the soil surface roughness by causing pedestalling or protrusions from the surface (Van Wesemael et al. 1996), which is not generally the case for nonrocky agricultural soils that usually exhibit a decreasing trend of soil surface roughness over time due to the breakdown of aggregates and subsequent sealing under rainfall. Exactly how the surface roughness responds to the change of rock cover, however, is unclear. Van Wesemael et al. (1996) investigated the surface roughness variations of soils containing rock fragments and found that, for soils containing small rock fragments, random roughness

Received May 21, 2019; Revised November 13, 2019; Accepted February 26, 2020.

Li Li is a PhD student in the School of Natural Resources and the Environment, University of Arizona, Tucson, Arizona. **Mark A. Nearing** is a research agricultural engineer, **Viktor O. Polyakov** is a soil scientist, **Mary H. Nichols** is research hydraulic engineer, and **Michelle L. Cavanaugh** is a hydrologic technician at the USDA Agricultural Research Service Southwest Watershed Research Center, Tucson, Arizona.

(RR) increased with rock cover to reach its maximum and then decreased. They further concluded that the changes of surface roughness corresponding to increasing rock covers were different for soils with small and large rock fragments. Surface roughness also can be altered by the erosional features, such as scour, depressions, plunge pool, or rills, which are produced by the localized flow around individual rocks (Abrahams et al. 1986; Bunte and Poesen 1993; Gómez and Nearing 2005; Rieke-Zapp et al. 2007). The development of those erosion features for surfaces with high rock cover percentage, however, are not as significant as for surfaces with low rock cover percentages due to the limited interrock spaces or rock protection (Bunte and Poesen 1993; Rieke-Zapp et al. 2007). Apparently, the existence of erosional features might complicate the commonly held perception that greater rock cover percentage is always associated with a rougher surface.

Contrasting results have been reported regarding the effects of soil surface roughness on runoff velocity. Usually, flow velocity has been assumed to decrease with increasing surface roughness. On the other hand, runoff may also concentrate around the roughness elements or in the rills on rough surfaces, thereby increasing the hydraulic radius of surface area and enhancing flow velocity (Helming et al. 1998; Ding and Huang 2017). Those opposing influences are further complicated by the flow characteristics. It has been widely recognized that the effects of roughness elements on flow velocity is a matter of protrusion or submergence of those elements; more specifically, the ratio of water depth to the roughness height is considered of importance. Holden et al. (2008) investigated the overland flow velocity properties in peatlands and found a significant "break" (a threshold of water depth around 1 cm) separating two hydraulic resistance curves. The hydraulic resistance first increased with flow depth as the surface first became fully submerged, and then decreased with increasing flow depth. It has been suggested by Parsons et al. (1990) that as overland flow traveled downslope, the flow was progressively concentrated into deeper threads that submerged surface roughness elements, leading to a decrease of hydraulic resistances. Hence, the effects of roughness elements on flow velocity and hydraulic resistance varied downslope with varying water depths.

The effects of rock cover percentage on hydraulic resistance have been studied on nonerodible surfaces (Gilley et al. 1992), paved desert surface (Abrahams et al. 1986; Nearing et al. 1999), and erodible surfaces with different rock cover percentage treatments (Bunte and Poesen 1993; Rieke-Zapp et al. 2007). However, there are a few contrasting results. Bunte and Poesen (1993) conducted flume experiments with rock cover ranging from 0% to 99% to investigate the effects of rock covers on erosion and transport of noncohesive sediment. They found that hydraulic resistance increased according to a monotonic power function with the increasing rock cover percentage. Their study, however, was limited to a highly erodible artificial surface, which does not fully reflect the conditions of natural surfaces. Rieke-Zapp et al. (2007) conducted laboratory flume experiments to investigate the effect of rock fragments on flow hydraulics. In the cases of initial surfaces with few or no rock fragments, the armoring effects by rock fragments were less effective, and significant headcuts or rills developed. The headcuts, in some cases, led to even greater overall hydraulic friction than the surfaces with higher rock covers.

Nearing et al. (2005) put forward a hypothesis of slope-velocity-equilibrium, that due to the feedback between erosion, surface morphology, and flow hydraulics, steeper areas develop a relative increase in surface physical roughness and hydraulic resistance, such that the greater downslope component of the gravitational acceleration [$g \times sin$(slope)] on steeper slope would be counteracted, resulting in an independence of flow velocity over slope gradients. In the hypothesis testing experiment of Nearing et al. (2017), 22 rainfall events were simulated on stony plots (2 × 6.1 m) with three slope treatments (20%, 12%, and 5%, two replications for each slope treatment). The total applied rainfall volume for each surface replication ranged from 1,400 to 2,240 mm, at relatively high intensity, to account for medium-term (ca. 10 years) rainfall erosion effects. The final surface random roughness values that were estimated from three transect measurements were different for each slope, and the final flow velocities measured on the evolved surfaces showed slope independence. However, given the limited transect measurements, interpretation of the experiment would benefit from denser surface measurements, enabling a closer inspection of the feedback between surface morphology and flow hydraulics. The present study is a continuation of Nearing et al. (2017) with the following objectives: (1) to provide more insight and detail of the spatiotemporal evolution of rock cover and surface roughness with aid of light detection and ranging (LiDAR) measurements; and (2) to investigate the relationships between rock cover, surface roughness, and flow velocity. The questions to be answered are how the surface roughness and flow velocity change as a function of the development of the rock pavement, and how the relationships differ as a function of rainfall intensity, slope gradient, and positions on the plot. Our results will benefit the improvement of process-based models, in which the parameters that define the state of the system and empirical relationship that quantify the interactions among subsystems should be updated for continuous simulations.

Materials and Methods

Soil Box and Rainfall Simulator. Experiments were conducted using a metal-bound box (6.1 by 2 m) that was described earlier by Nearing et al. (2017). The slope was adjustable, ranging from 0% to 20%. Slope gradients of 5%, 12%, and 20% slope were utilized in this study. Each slope was replicated; hence six experiments in total were conducted. Rainfall was simulated by a Walnut Gulch Rainfall Simulator that was described by Paige et al. (2004). By controlling the spray time of nozzles, which were mounted on a computer-programmed oscillating boom, various rainfall rates ranging from 13 to 190 mm h^{-1} with a kinetic energy of approximately 204 kJ ha^{-1} mm^{-1} could be obtained on a 6.1 by 2 m area. Windscreens were constructed surrounding the soil box to minimize unwanted wind disturbance.

Rainfall Applications and Velocity Measurements. The soil box was first positioned horizontally to fill with soil to a depth of 20 cm for each experiment. A wooden board was used to even the soil surface. The soil surface was then prewet with 35 mm h^{-1} intensity of rainfall for 30 minutes to create a relatively consistent initial moisture condition. The box was then adjusted to the designated slope (5%, 12%, or 20%).

The velocity was measured by using a salt tracer (Nearing et al. 2017; Polyakov et al. 2018b). Two liters of salt tracer was uniformly applied using a perforated PVC pipe

Figure 1
The experimental plot and LiDAR scanning positions (number in the circle indicates the position number). Control points were used for scan-to-scan registrations. Bold dashed lines indicate the positions where salt tracer was introduced to measure flow velocities. The sensors used to measure flow electrical resistivity were embedded in the lower edge of the plot. Three sections, namely lower, middle and upper, were defined.

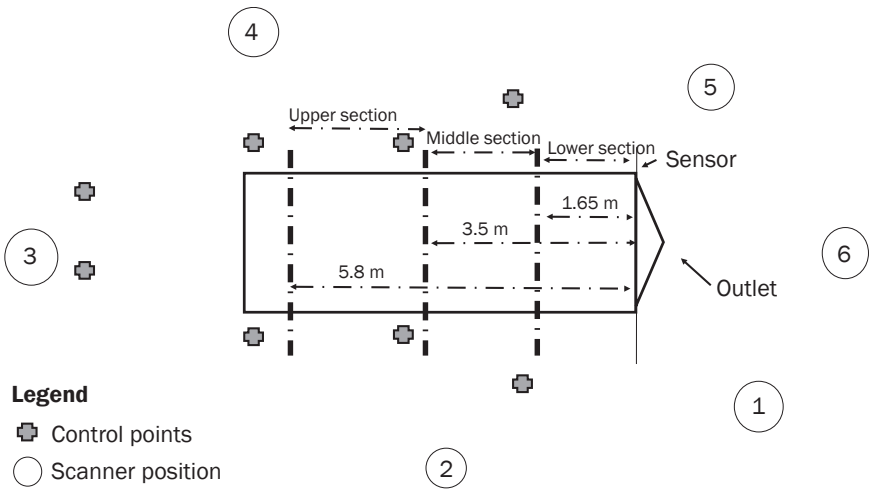

across the plot crossing three travel distances, which were 1.65, 3.5, and 5.8 m from the outlet (figure 1). Sensors embedded in the edge of the flume at the end of the plot were deployed to measure the runoff electrical resistivity, which was immediately recorded by using LoggerNet software and CR10X data logger by Campbell Scientific. The measured data were stored in a real-time graphical format with resolution of 0.37 s. The mean velocity used the arrival time of the peak concentration since the peak values from the salt curve (Polyakov et al. 2018b) were found to be more reliable (Nearing et al. 2017). We hereafter considered 0 to 1.65, 1.65 to 3.5, and 3.5 to 5.8 m as the lower, middle, and upper sections of the plots, respectively (figure 1).

The velocities for the middle section were calculated from the measured velocities at 3.5 m and adjusted for the velocities measured for the lower section (measured at 1.65 m). Similarly, the velocities for the upper section were calculated from the measured velocities at 5.8 m and adjusted using the velocities measured at 3.5 m.

Considering that the shallower slope did not evolve as rapidly as did the steeper slope, rainfall was simulated three times for the 20% slope, while simulated four times for 12% and 5% slopes. Each simulation was considered as a continuous rainfall application with duration time ranging from 1.5 to 5 hours. The detailed procedures of rainfall application were documented in Nearing et al. (2017). For each experiment (replication), the first rainfall simulation was started with low intensity (59 mm h^{-1}). Once runoff reached steady state, flow velocity measurements at low intensity (59 mm h^{-1}) were conducted over the three distances starting from the lower section. Rainfall intensity then was raised to 178 mm h^{-1}, with another set of velocity measurements at high rainfall intensity. After approximately 1 hour rainfall application, flow velocities were measured again at high (178 mm h^{-1}) and low (59 mm h^{-1}) rainfall intensities. Subsequent simulations were started from high intensity (178 mm h^{-1}) for most of the simulation time with a set of velocity measurements at the end. Rainfall intensity then was decreased to 59 mm h^{-1}, and the velocity measurements were repeated at the end of rainfall application.

A precalibrated V-shaped flume equipped with an electronic depth gate was used to measure the runoff discharge. The flume was also calibrated and verified using weighed runoff collected in buckets intermittently during the simulations. Runoff samples were oven dried in the lab after rainfall experiments and used for determining the sediment concentration. When all simulations of an experiment were completed, the topsoil layer was removed and replaced by the fresh soil.

Rock Fragment Cover. The surface rock cover was measured with a transparent, handheld size guide used before each simulation and after the last simulation for each experimental replication at 300 points on a 20 by 20 cm grid. The guide helped to objectively determine if rock was present on the surface (>0.5 cm and 0.5 to 1.0 cm). A rail on which a laser pointer was moved in steps of 20 cm was positioned across the plot for each row of the measurements. The downward pointing laser beam identified the sample point locations to ensure the surface rock was measured at the same point every time. The sample points with measurements that were greater than 0.5 cm (Poesen et al. 1998) were considered as rock and counted for calculating the rock fragment cover percentage.

Soil Surface Random Roughness. Soil surface elevation information were sampled using RIEGL VZ400 terrestrial LiDAR before each simulation and after the last simulation for each experimental replication. A laser beam with a nominal divergence of 0.3 mrad (corresponding to an increase of 30 mm of beam diameter per 100 m distance) was emitted by the instrument to measure the surface elevation quickly and with high precision. Six scanning positions were set up around the surface (figure 1) to minimize the occlusions effects of rocks. Eight control points were established around the soil box (figure 1), and their coordinates were surveyed with a Trimble R8 robotic total station. Eight cylindrical reflectors with diameters of 10 cm were installed over the control points on survey tripods to register the six scans into a composite point cloud. Procedural details of scan-to-scan registration are available (Li et al. 2019).

Approximately 23, 23, 26, and 10 cm of the left, right, upper, and lower of the box outer edges, respectively, were omitted from the composite point clouds to minimize the boundary effects of the soil box borders, resulting in a LiDAR point cloud covering an area of approximately 5.63 m by 1.53 m. In total, 560 transects crossing the plot were selected for each surface at an interval of 1 cm up and down the plot. Five hundred sixty straight lines crossing the plot horizontally at a separation distance of 1 cm apart were defined. Each line then was treated as the center line of a band with 2 mm width. The LiDAR points that fell into each 2 mm wide band were first linearly detrended to eliminate the slope effects and then used to

calculate the RR for that band using the following formula:

$$RR = \sqrt{\frac{1}{N}\sum_{j=1}^{N}(Z_j - \bar{Z})^2} \quad , \qquad (1)$$

where RR is surface random roughness of each band, N is the number of the measurements, Z_j is the elevation measurement at point j, and $\bar{Z}$ is the average value of those N measurements. Means (hereafter referred to as ARR) and variations of the RR values of all the transects on the full plot and in each plot section were calculated.

Soil Surface Transects Measurements. Three additional transects across the plot at 0.9, 2.9, and 4.9 m from the lower edge of the plot were selected for measurement by a laser elevation meter. Surface elevation was measured using a Leica3 E7500i laser distance meter with a resolution of 5 mm for each transect. The accuracy of measurement was ±0.2 mm. Details of this laser equipment were presented in Polyakov and Nearing (2019). Transect measurements were conducted before each simulation and after the last simulation, as near as possible to the timing of the velocity measurements.

Data Analysis. Darcy-Weisbach hydraulic factor was calculated using the standard equation:

$$f = \frac{8gds}{v^2} \quad , \qquad (2)$$

where f is hydraulic factor (dimensionless), g is the acceleration due to gravity (9.8 m s^{-2}), d is the water depth (m), S is the bed surface slope (m m^{-1}), and v is the flow velocity (m s^{-1}).

The relationship between the rock cover and RR was developed using the measured data, while the relationships involving the velocity were made using interpolated values of rock covers and RR based on the timing during the rainfall of the velocity measurements relative to the timing of rock cover and RR measurements. Differences reported in this paper are based on $p = 0.05$. We refer to the "initial surface" as the surface after prewetting but before actual rainfall application; "terminal rock cover" and "terminal velocity" refer to the rock cover and flow velocity measured at the end of experiments.

Results and Discussion

Runoff and Sediment Load. The duration of rainfall application, cumulative runoff, measured sediment load, and calculated erosion rate for each simulation are shown in table 1. The first simulation for each experimental replication lasted for 1.5 to 2 hours, and the duration of subsequent rainfall applications increased up to 5 hours, hence the concomitant increasing cumulative runoff. Erosion rates continually decreased during a given experimental replication, probably due to the increases of rock cover and surface roughness over time (discussed below) that tended to protect the soil surface, retard flow velocity, and dissipate flow energy.

The Evolution of Rock Cover. Rock cover (>0.5 cm) as a function of cumulative runoff for the full plot and each section (lower, middle, and upper) is plotted in figure 2. We intended to create relatively constant and uniform initial surface conditions for each replication, which was difficult. The initial rock cover ranged from 15% (for replication 1 of 20% slope) to 41% (for replication 2 of

Table 1
The rainfall duration, cumulative runoff, sediment load, and calculated erosion rate of each simulation for two replications at 20%, 12%, and 5% slopes.

Slope (%)	Replication	Simulation	Duration (min)	Cumulative runoff (mm)	Sediment load (kg)	Erosion rate (kg m^{-2} min^{-1})	Average erosion rate (kg m^{-2} min^{-1})
20	1	1	94	140	94	0.083	0.041
		2	148	333	77	0.044	
		3	314	718	78	0.021	
	2	1	113	164	66	0.048	
		2	155	338	59	0.032	
		3	324	788	70	0.018	
12	1	1	107	169	86	0.067	0.027
		2	169	387	82	0.041	
		3	289	737	69	0.020	
		4	287	698	33	0.010	
	2	1	126	191	54	0.036	
		2	172	359	43	0.021	
		3	299	651	39	0.011	
		4	305	742	36	0.010	
5	1	1	141	223	38	0.022	0.014
		2	195	412	41	0.017	
		3	258	586	29	0.010	
		4	302	698	25	0.007	
	2	1	134	211	38	0.024	
		2	209	409	33	0.013	
		3	265	648	34	0.011	
		4	309	752	28	0.008	

Figure 2
Rock cover (>0.5 cm) as a function of cumulative runoff for the (a) full plot, (b) lower, (c) middle, and (d) upper sections.

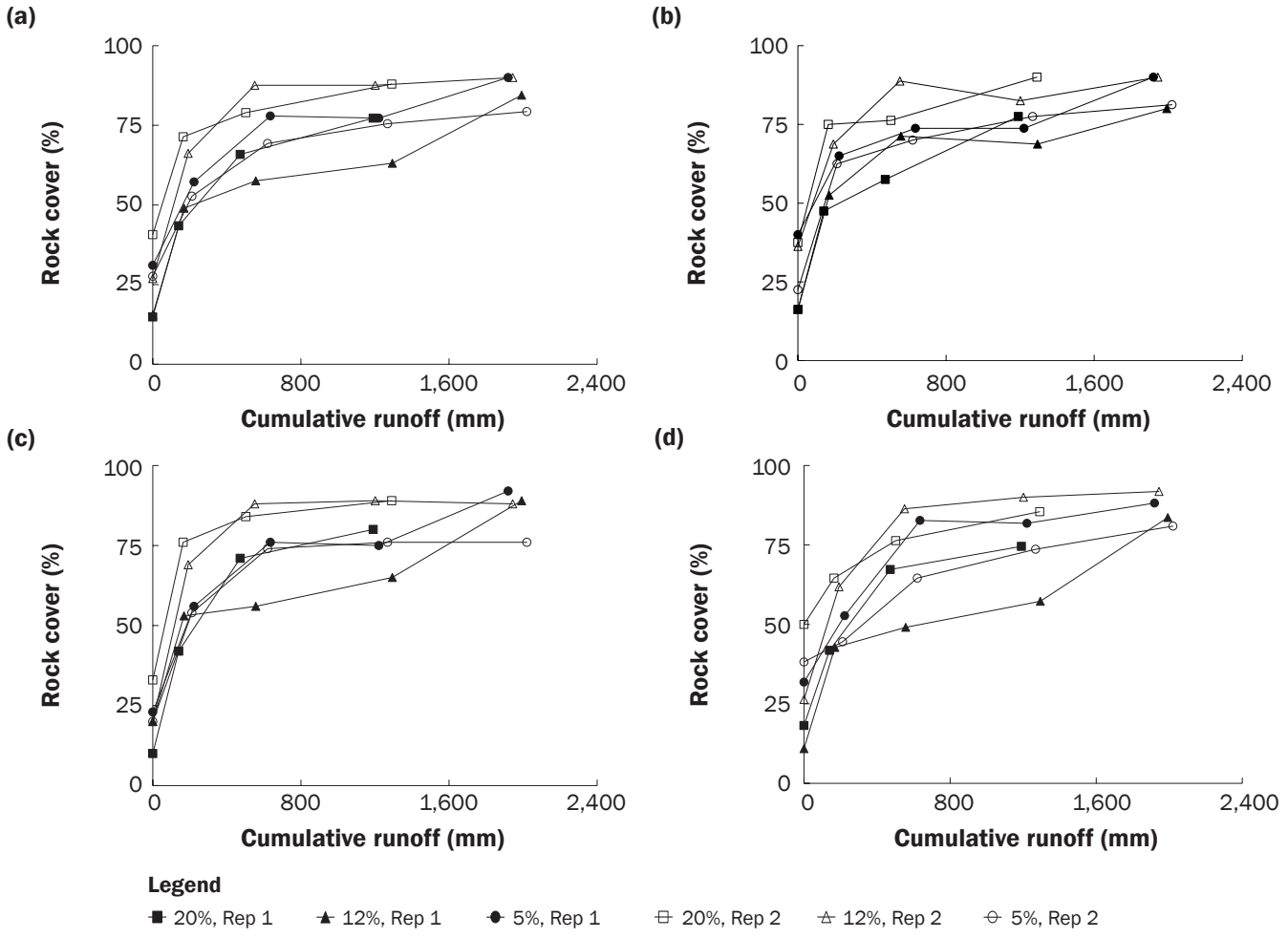

20% slope) for the full plot scale (figure 2a). As rainfall progressed, the rock covers displayed increasing trends, with final rock covers of up to 90% at the end of experiment. The terminal rock cover of the full plot did not show slope dependency (as was also indicated in Nearing et al. [2017]). Rock covers exhibited increasing trends as cumulative runoff also increased (figures 2b, 2c, and 2d) for each of the sections. However, there were no consistent differences of rock cover amongst the lower, middle, and upper plot sections.

The fact that rock fragments became concentrated on the surface was resultant from the selective removal of fine materials (and possibly very small rock fragments) either by raindrop splash, interrill, or rill erosion (Shaw 1929). Thus variations of rock cover in nature as an erosional product of soils containing rock fragments may result from the differences of erosion rate (Simanton and Toy 1994; Poesen et al. 1998). Our data showed (figure 3) that greater erosion rates for each simulation tended to result in greater changes of rock cover during the rainfall simulation.

Our results showed that the rock cover was not slope dependent, which does not support the previous findings that steeper slopes were associated with greater rock covers (Simanton and Toy 1994; Simanton et al. 1994; Poesen et al. 1998). Nearing et al. (2017) concluded that this independence was resultant from the fact that the evolved surfaces in the experiments were at maximum coverage possible for the experimental soil under natural hillslope conditions. Another possible reason was the incision of rills. Rock covers in the studies of Simanton and Toy (1994), Simanton et al. (1994), and Poesen et al. (1998) were measured specifically from selected interrill areas on hillslope segments without apparent concentrated flow path or rills, and with no or sparse vegetation. One may imagine that in the case in which interrill erosion solely occurs, continued exhumations of rock fragment are required to dissipate flow energy; hence the rock cover on the steeper slope would be greater in order to provide sufficient armoring effects.

For the case when both rill and interrill erosion occur, development of headcuts and step-pool structures in the rills could also offer comparable retarding effects (Govers 1992; Nearing et al. 1999; Giménez et al. 2004; Rieke-Zapp et al. 2007). Steeper slopes, moreover, will be more likely to initiate rilling in the early stage of rainfall events if the initial surface is covered by few rock fragments and is characterized with low surface roughness. In our experiment, it appears that development of more pronounced rills occurred on the steeper slopes compared to the shallower slopes (discussed

Figure 3
The change of rock cover (full plot) for each simulation of each slope treatment as a function of erosion rate using data from table 1.

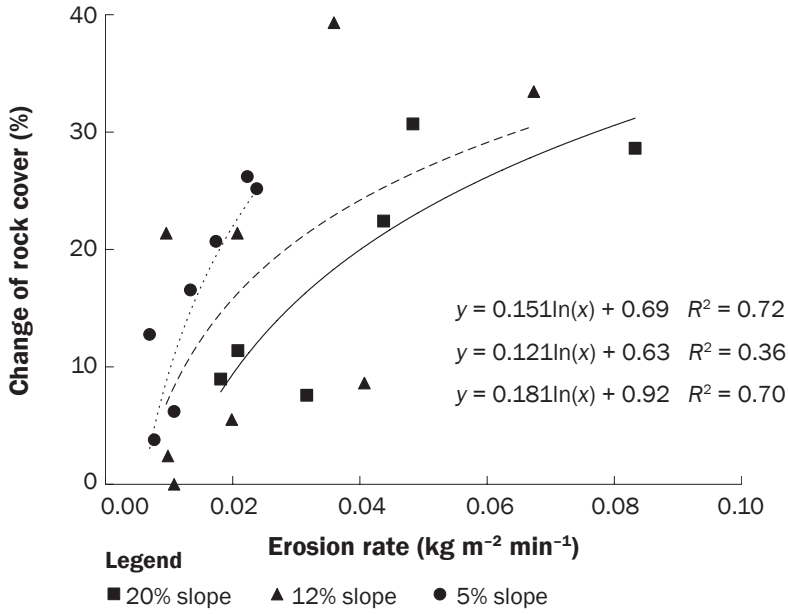

below). We propose that in the experiment part of the energy dissipation occurs in rills and headcuts, partially explaining the lack of relationship between slope gradient and terminal rock cover. This might also explain why the erosion-induced rock cover changes on 20% slope tended to be lower for a given erosion rate (figure 3).

Another factor that contributed to this independence of final rock cover and slope might be that rock fragments eroded in the upper section may be trapped or deposited in the middle or lower section on a gentle slope instead of being delivered to the outlet due to the incompetence of the interrill flow for transporting the coarser fractions (Parsons et al. 1991), potentially enhancing the rock covers on shallow slopes (Poesen et al. 1998). On natural hillslopes, the logarithmic relationship between hillslope gradient and rock fragment cover also does not hold true for all cases, due to the influences of slope aspects, tillage practices, lithology, and vegetation (Poesen et al. 1998; Polyakov et al. 2018a). For example, Polyakov et al. (2018a) analyzed plot data collected on 20 rangeland sites in Arizona and Nevada from 2006 to 2013. They concluded that both the biotic and abiotic factors, including the slope gradient, soil compactions, vegetation, and microbiological activity contributed to the terminal rock cover.

We initially expected that the formation of rock pavement in the upper section would require longer rainfall applications or not be as significant as in the lower and middle section. However, there were no consistent differences of rock cover amongst the lower, middle, and upper sections with the simulated rainfalls. One reason for this may be related to splash detachment. Of course, there is no way to use our data to differentiate and quantify the splash erosion, but a speculation may be drawn referring to Torri et al. (1987). Their data clearly showed that the raindrop detaching power was dispersed by the water layer—the greater the water depth, the more the splash detachment capacity was dissipated. The effect of runoff depth on splash detachment was quantitatively incorporated into the European Soil Erosion Model (Torri and Poesen 1992). It is possible that water depth in the upper section was lower than that in the middle and lower sections. The rock fragments exposed by detachment of raindrops in the upper section, moreover, were unlikely to be as easily transported by overland flow as in the middle and lower sections due to relatively low flow velocity and transport capacity.

Soil Surface Random Roughness of the Full Plot. Figure 4 shows the temporal variations of ARR of full plots for each experimental replication. The initial ARR ranged from 2.2 to 2.9 mm, the variations of which were primarily due to different numbers of rocks exposed on the initial surfaces. As rainfall progressed, ARR predominantly displayed increasing trends with some exceptions, for example, the decrease of ARR for replication 1 of 5% slope during the first simulation, and the insignificant increase of ARR for replication 1 of 20% slope during the second simulation. The terminal ARR values were 5.3 and 5.1 mm, 4.2 and 4.5 mm, and 2.9 and 3.2 mm for replications of 20%, 12%, and 5% slopes, respectively. Figure 4 also shows that for each surface there was a large variability (wide range between 25% and 75% percentile) of RR among those 560 transects, connoting that on the stony surfaces, a limited number of transects might not be enough to characterize the soil surface roughness due to the random position and size of rock fragments and spatial variations of RR. The number of transects required to obtain a "representative" ARR (Bryant et al. 2007) on stony surfaces is worthy of further investigation. Our results derived from very dense surface measurements clearly showed that the steeper slopes produced rougher surfaces, which fully supported the theory of slope-velocity equilibrium (Nearing et al. 2017).

Soil Surface Random Roughness of Each Section. The changes of ARR in the upper section over time is shown in figure 5. ARR mainly followed increasing trends on 20% and 12% slopes, while on 5% slope, the surfaces did not change significantly during the early simulations but became rougher under further rainfall applications. The terminal ARR in the upper section were greatest on 20% slope, then 12% and 5% slope with values of 4.7 and 4.6, 4.3 and 4.5, and 3.1 and 3.2 mm, respectively.

The ARRs of the middle section gradually increased over time with exceptions for replication 1 both on 20% and 12% slopes, for which ARR increased by a large amount in the first simulation and then gradually increased by small amounts during subsequent simulations (figure 6). The 20% slope developed rougher surfaces in the middle section at the end of experiments with ARR values of 5.7 and 5.4 mm for the two replications.

The temporal variations of ARR in the lower section were much different than those found in the middle and upper section (figure 7). ARR tended to decrease first and then increase for the two replications on 5% slope. Surfaces for replication 2 of 12% slope did not significantly evolve over time except

Figure 4
Surface random roughness as a function of cumulative runoff for full plot. *N* and μ indicates the number of transects for calculating the random roughness and the average random roughness, respectively. "I*" represents significant increase. "D*" represents significant decrease.

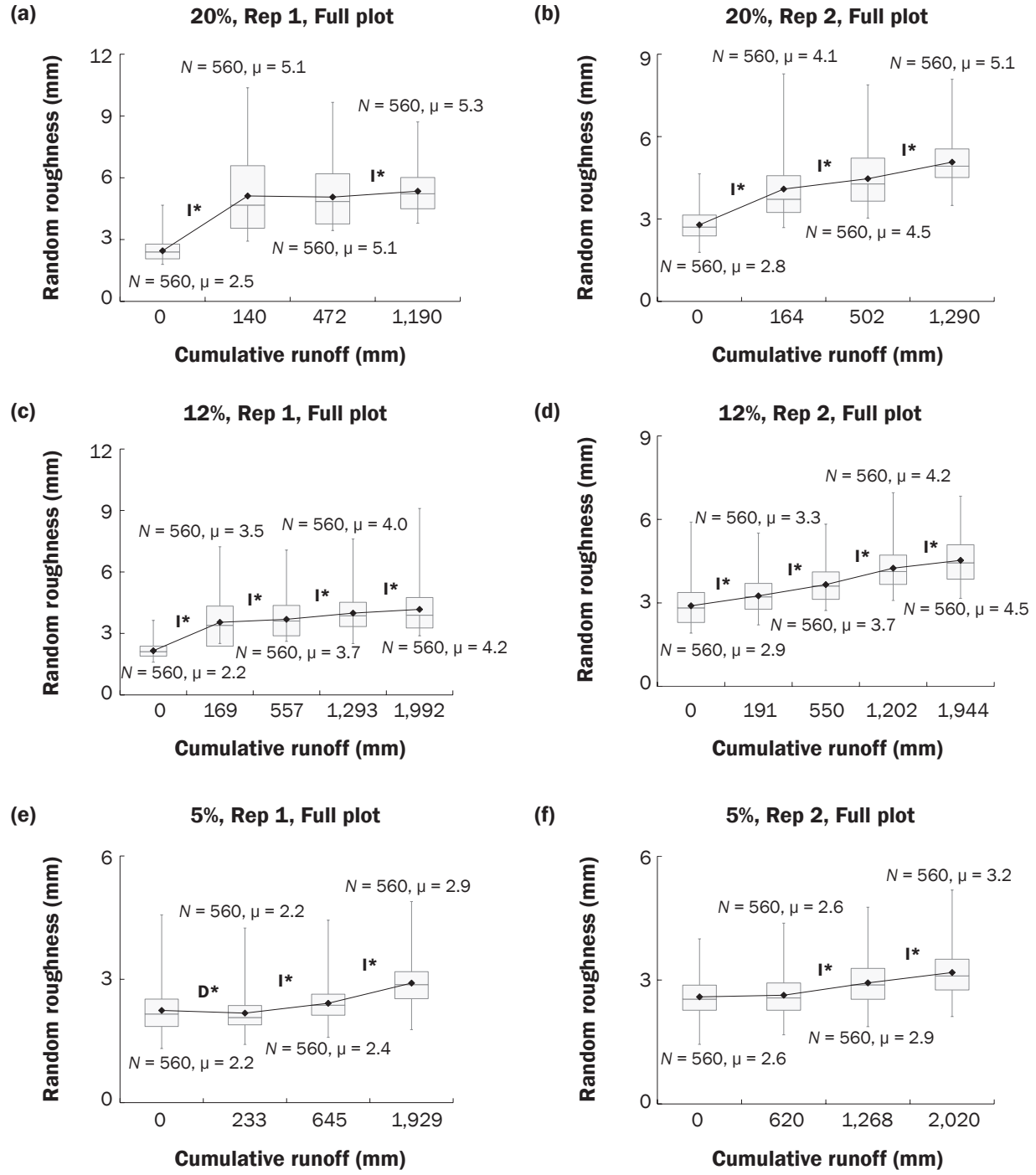

for an increase of ARR during the third simulation. The first simulation produced very pronounced increases of ARR for replication 1 on both 20% and 12% slopes, while the subsequent simulations continually caused decreases of ARR. Those decreases of ARR in the lower section were counter to the increasing ARRs in the middle and upper sections, leading to a small amount of increase in ARR for the full plot (figure 4). ARR for replication 2 of 20% also remarkably increased after the first simulation, and decreased by a small amount during the subsequent simulations. Though in the lower section different temporal trends of ARR

Figure 5
Surface random roughness as a function of cumulative runoff for upper plot sections. *N* and μ indicates the number of transects for calculating the random roughness and the average random roughness, respectively. "I*" represents significant increase.

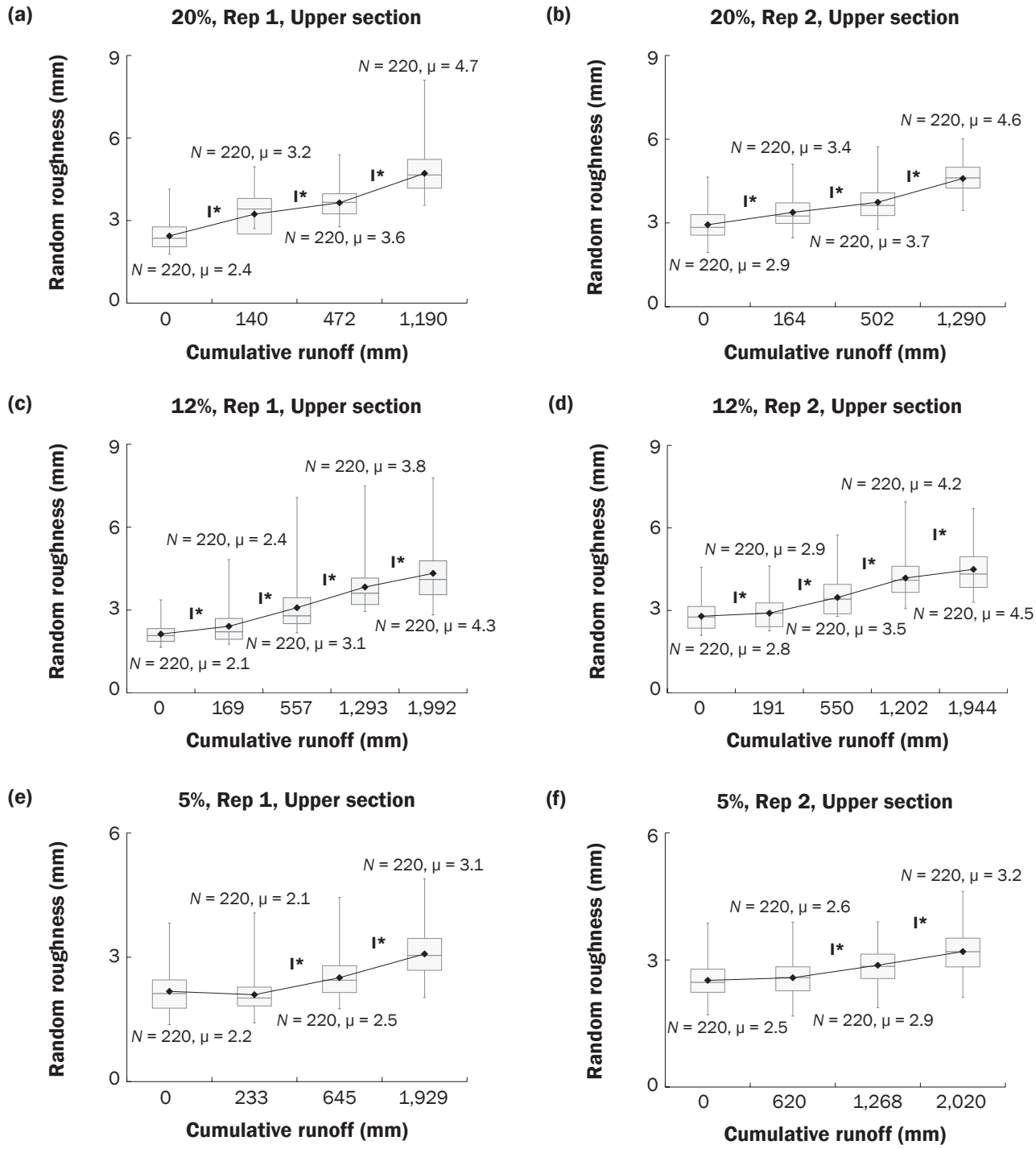

were exhibited among the six experiments, the greatest terminal ARR values were found on 20% slope and lowest on 5% slope.

There were no consistent differences in the terminal roughness on the upper, middle, and lower sections for each slope treatment.

The Influences of Rock Cover on Soil Surface Random Roughness. The common perception that greater rock cover is always associated with greater surface roughness does not hold true for all cases in our study, especially in the lower section where surface roughness did not uniformly increase

Figure 6
Surface random roughness as a function of cumulative runoff for middle plot sections. *N* and μ indicates the number of transects for calculating the random roughness and the average random roughness, respectively. "I*" represents significant increase.

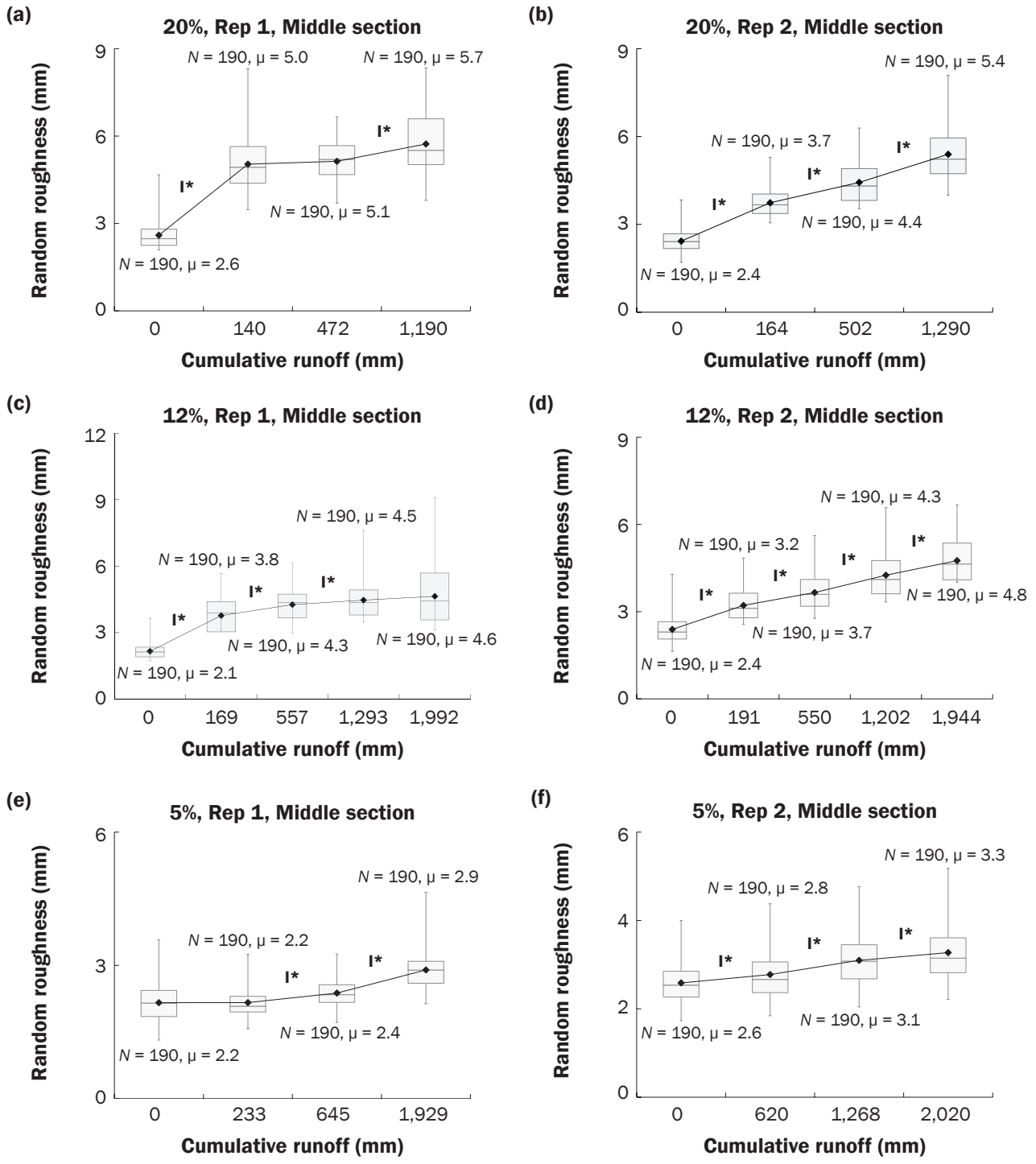

with increasing rock cover (figures 7 and 2). Figure 8 shows ARR as a function of rock cover for the full plot and each section. Significant correlation between ARR and rock cover on 5% slope was only found in the upper section. ARR was not significantly correlated with rock cover in the lower section on 20%, 12%, and 5% slopes. The decreases of ARR in the early rainfall stages on 5% slope were likely due to the smoothing effects from surface sealing or deposition of splashed particles that traveled in short distances. However, the following two questions are raised by this: (1) why in the lower section did ARR not significantly correlate

Figure 7
Surface random roughness as a function of cumulative runoff for lower plot sections. *N* and μ indicates the number of transects for calculating the random roughness and the average random roughness, respectively. "I*" represents significant increase. "D*" represents significant decrease.

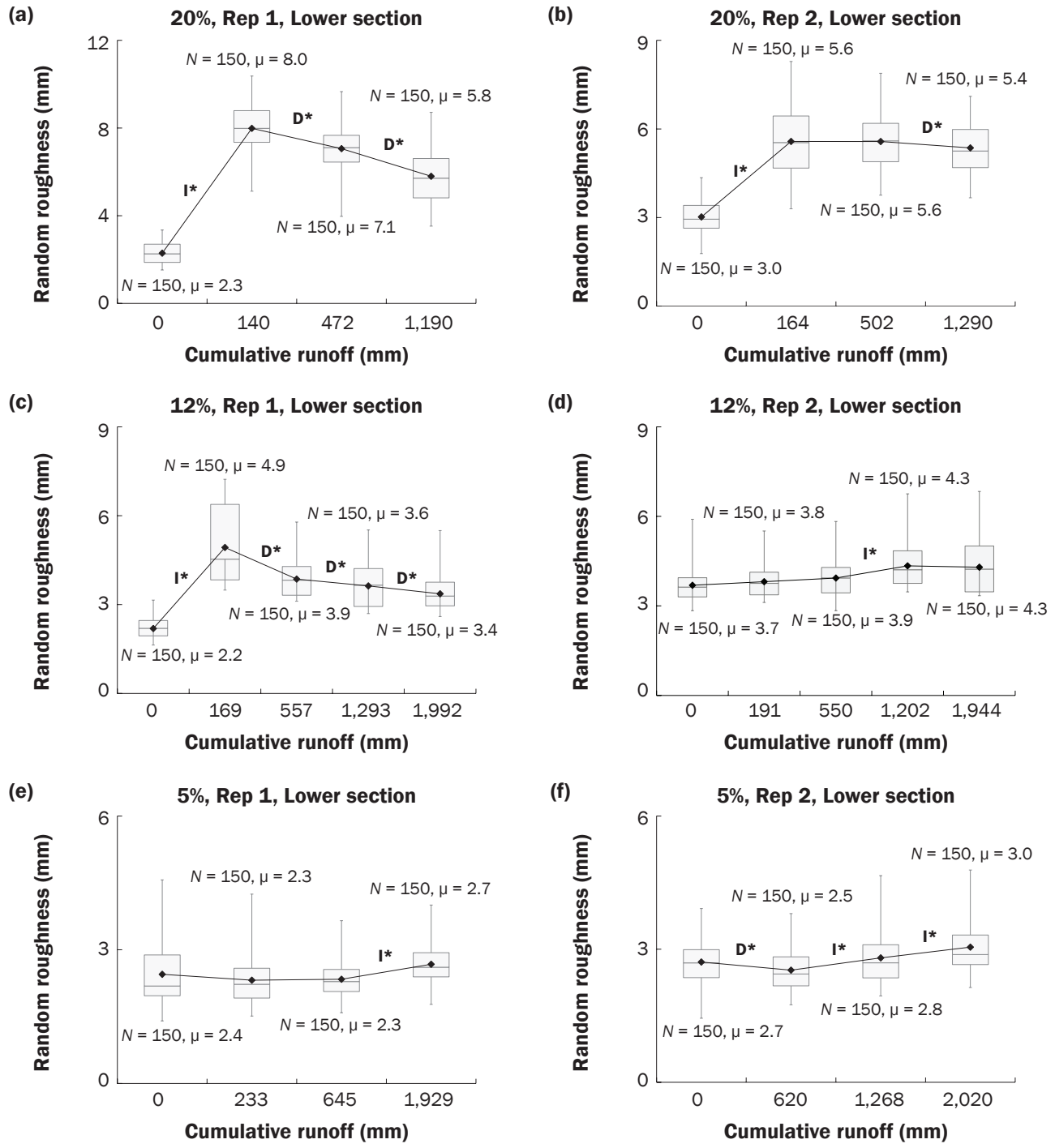

with rock cover, and (2) why did the roughness tend to be greater on the steeper slope in the middle and upper sections given the fact that rock covers were not significantly different among the slope treatments?

The first question might be explainable by the existence of rills that quickly formed in the early rainfall simulations. Figure 9 shows the changes of the soil surface cross-section (0.9 m from the lower edge of the plot) in the lower section after the first simulation for the two replications of 12% and 20% slope. Rills were formed at two replications of 20% slope and replication 1 of 12% slope compared with initial surfaces, which increased the RR of the lower section from 2.3 to 8.0 mm, 3.0 to 5.6 mm, and 2.2 to 4.9 mm,

Figure 8
Average random roughness as a function of rock cover for (a) full plot, (b) upper, (c) middle, and (d) lower plot sections.

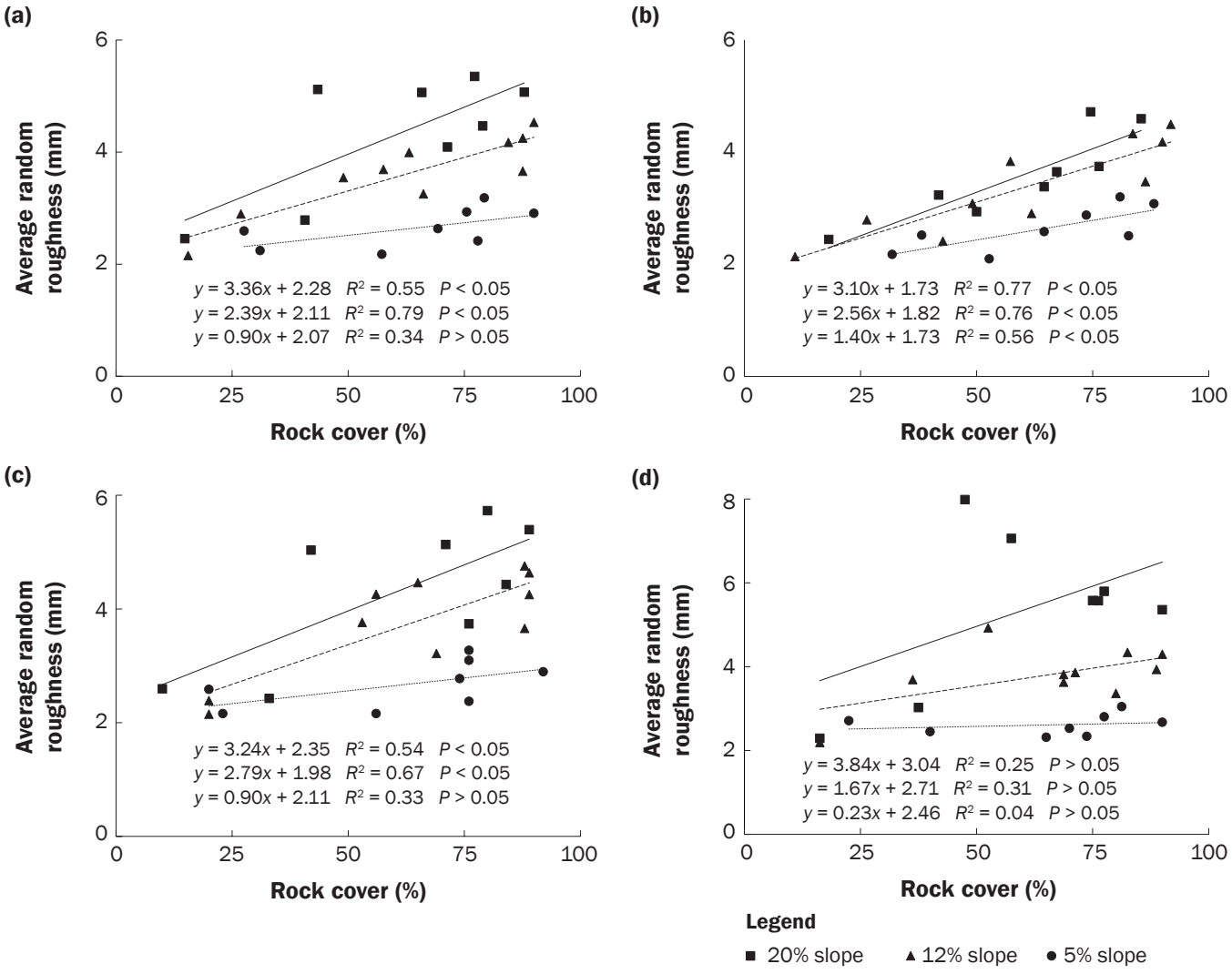

respectively (figure 7). No apparent rills were found for replication 2 of 12% slope, which is likely due the greater initial rock cover and surface roughness (figure 7), and the ARR did not, therefore, significantly change. The decreases of ARR for two replications on 20% and replication 1 on 12% slope during the subsequent rainfall simulations (figure 7) might be because of the geometric changes of the rills. Figure 10 gives the elevation changes of the profiles in the lower sections after the first and third simulation for replication 1 of 20% slope as an example. The width of the already formed narrow rills in the first simulation widened over time, due to the sidewall sloughing after three simulations, as indicated from A1 to A2, or from B1 to B2. As the width of rills enlarged, a few rills connected and developed into large depressions (for example, D1), hence the greater variations of surface elevations caused by the few deep rills diminished, leading to decreases of roughness for the lower section as a whole. Therefore, in the case of rill incision, the variations of roughness were dominantly controlled by the changes of form roughness (rills or depressions) rather than the changes of rock cover, hence the ambiguity between rock cover and surface roughness.

The second question might be addressed by erosion-induced variations of surface microtopography. For example, around the rocks, "hoof-print depression" might develop (Poesen and Lavee 1994), and their dimensions would be related with erosion potentials and flow discharges (Bunte and Poesen 1993).

Those erosion features (including rills), as aforementioned, would blur the relationship between rock percentage and surface roughness, which is seen here in that the determination coefficients (r^2) decreased downslope from upper plot sections to the lower sections (figure 8) as erosion features became more pronounced. We conclude here that the changes of rock cover did not fully explain the variations of surface roughness. Nevertheless, this result does not violate the theory of slope-velocity equilibrium that steeper slopes have a greater terminal surface roughness.

The Temporal Changes of Flow Velocity. Flow velocity as a function of cumulative runoff under rainfall intensities of

Figure 9
Surface elevations of the lower transect (0.9 m from the outlet) before and after the first rainfall simulation for 20% and 12% slopes.

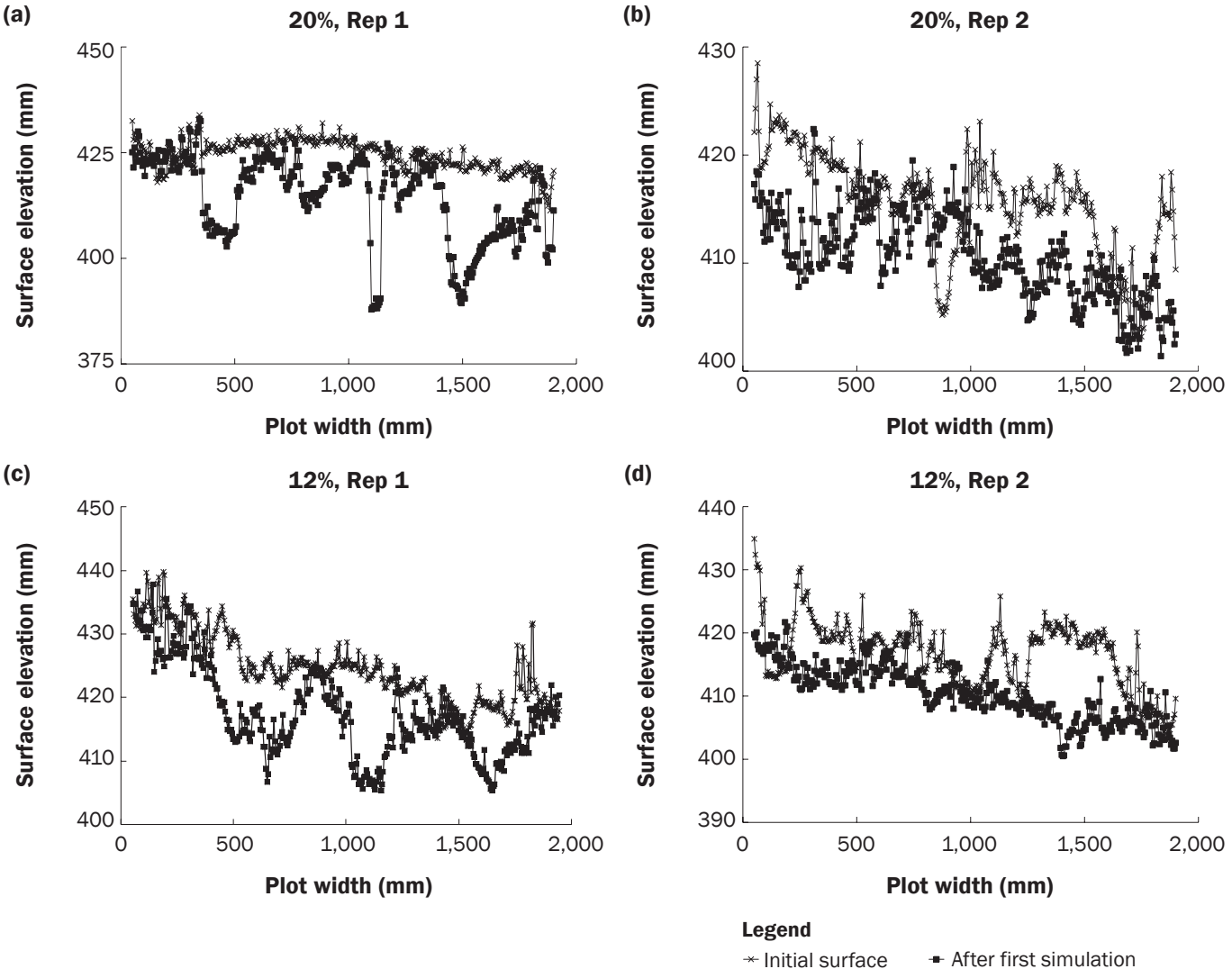

59 (referred to as "low") and 178 mm h^{-1} (referred to as "high") is shown in figure 11. The initial values of flow velocity tended to be greater on the steeper slopes and under greater rainfall intensity. Flow velocities primarily decreased as rainfall progressed. However, some anomalies were found in the lower section where on 12% and 20% slopes the flow velocities rapidly increased in the first simulation and then decreased in the subsequent rainfall applications. Setting aside those anomalies, the terminal velocities tended to reach relatively constant values, which were unaffected by slope, approximately 0.037, 0.027, and 0.013 m s^{-1} under low rainfall intensity, and 0.065, 0.057, and 0.028 m s^{-1} under high rainfall intensity, for the lower, middle, and upper sections, respectively. These results supported the slope-velocity-equilibrium hypothesis that flow velocities on the evolved surface (terminal velocity) will be dependent on the flow discharge rates (Nearing et al. 2017), which is consistent with previous studies that either concentrated flow in rills (Govers 1992) or overland flow on 20 rangeland sites crossing the southwest United States (Polyakov et al. 2018a). The best-fit power relationship is showed in figure 12.

The Influences of Rock Cover and Random Roughness on Flow Velocities. Given the fact that no apparent rills were found in the upper and middle sections, and that rock cover and RR continually increased over rainfalls, the overall decreasing trends of flow velocity were therefore mainly due to the retarding effects imposed by dynamic changes of rock cover and RR. This is seen in figure 13 wherein flow velocities decreased following power functions with increasing RR (or rock cover). Rock cover better explains the variability of flow velocities than does RR, as quantified by the determination coefficients of power functions.

In the study of Bunte and Poesen (1993), a power function was also given to quantify the effects of rock cover percentage on flow velocity. They found that for a constant dis-

Figure 10
Surface elevations of the lower transect (0.9 m from the outlet) for rainfall simulations at replication 1 of 20% slope. Positions A1, A2, B1, and B2 shown in the graph were visually identified as rills. D1 was visually considered as a depression.

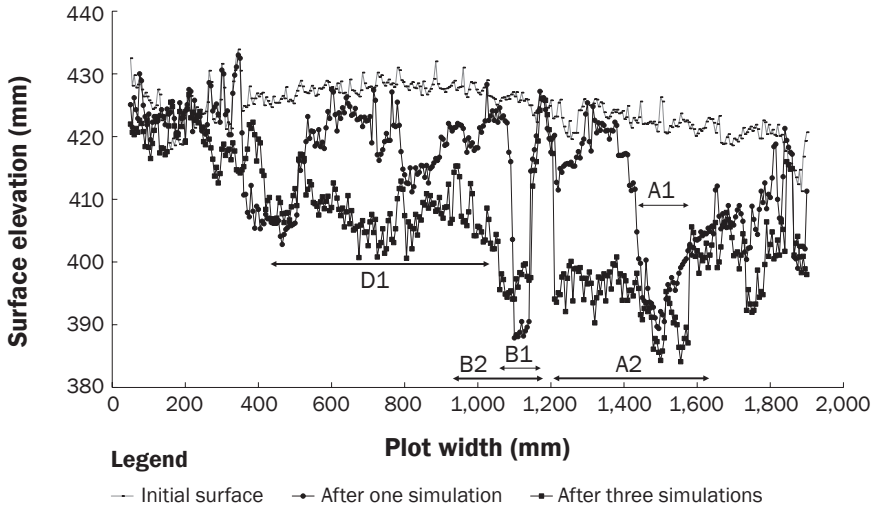

charge, a drastic decrease of flow velocities occurred as the rock cover percentage was increased from 0% to 20%, with slight reductions of velocity with further increased rock cover percentage. However, the reductions of flow velocity were more apparent when rock cover reached up to approximately 65% to 75% in our study, which are the typical values of rock cover found on many hillslopes (Abrahams and Parsons 1994). Those differences might be because the experimental soils in Bunte and Poesen (1993) were highly erodible sands, and the flow energy was fast spent in the formation of scours around the rock elements. In our study, however, in the upper and middle sections where no apparent rills incised, more rock cover was required to dissipate the flow energy, thus retarding the flow.

Steeper slopes and the upper sections tended to have greater hydraulic resistances for a given surface condition (in terms of both RR and rock cover) (figure 14). Pearson correlation coefficients (figure 14) indicated that hydraulic resistances were strongly correlated with slope gradient, rock cover, surface roughness, and especially with discharge rate. Multiple regression analyses were performed, and a hydraulic resistance prediction model is given in figure 14e. It is quite interesting to note that rock cover and slope gradient entered into the regression model while the RR term was excluded. This is likely because the RR was collinear with rock cover and slope gradient. The differences between our equation with those equations provided by Abrahams and Parsons (1991) are due to the following: (1) their experiments were conducted on previously paved surfaces while our experiments transitioned from initial surfaces with few rocks to the final paved surfaces; (2) the differences of hydraulic resistances caused by the different methods for generating overland flow (rain-induced versus trickle-induced) (Parsons et al. 1994).

The slope effects on hydraulic resistance are not surprising since slope as a term entered into the formula to calculate hydraulic resistance, and steeper slopes have a greater surface roughness. The flow rate in the middle sections was greater than that of upper sections in all cases, which results in a greater Reynold number (*Re*) (Parsons et al. 1990). A negatively sloping relationship between *f*-*Re* was reported previously for rock-paved surfaces (Abrahams and Parsons 1991, 1994), which resulted from the progressive inundation of the surface with increasing flow depth. Compared with experiments in which rocks were glued on the nonerodible flume (Gilley et al. 1992), the inundation ratio of roughness elements on natural stony plots is more difficult to quantify since the size and shape of roughness elements, and flow depth spatially varied. Two processes operate simultaneously to affect the flow resistance as *Re* increases, according to Abrahams et al. (1986). For one, the form resistance increases with the increasing wetted upstream-projected areas when more roughness elements are inundated. Secondly, the resistance of already fully submerged roughness elements will decrease as water depth increases. It would be anticipated that the first process will be dominant under low flow discharge (upper sections and low rainfall intensity in our case) and the latter process dominates in greater flow discharge conditions (middle section and high rainfall intensity in our case). Note that hydraulic resistances under low rainfall intensity were greater than those under high rainfall intensity, which is due to the different runoff rates. This was not the result found in previous studies on nonerodible surfaces that compared the rainfall resistance of raindrops (Li 2009).

Because of the existence of rills in the lower section, we did not attempt here to develop regressions between flow velocity (and hydraulic resistance) with RR. We speculate that the increases of flow velocity in the lower section (figures 11a and 11b) during the first simulation were because flow was more concentrated in the rills rather than moving as sheet flow. The increased water depth rapidly submerged the roughness elements on the rill beds, hence the flow was more hydraulically efficient with increasing depth of flow. The RR decreased during subsequent simulations while the velocity also decreased. We propose that this phenomenon may be explained by (1) the increases of rock covers that acted to reduce flow velocity (figure 2b) and (2) the geometric changes of rills and concomitant changes of flow width and depth (figure 10). Those changes would seem to have apparent importance for understanding the decrease of flow velocity. On one hand, flow was not as concentrated as in the first simulation but more spread out; hence flow crossed more roughness elements. On other hand, the increase of flow width led to a decrease of water depth. For those roughness elements fully submerged, decreasing water depth resulted in an increase of hydraulic resistance, hence the reductions of velocity. Finally, (3) the step-pools and headcuts along the rills could also retard the water flow (Govers 1992; Nearing et al. 1999; Rieke-Zapp et al. 2007). Our speculations would benefit from simultaneous water depth measurements to characterize the wetted cross section.

We note that the hydraulic prediction model given in figure 14e excluded the roughness term but included rock cover, and that only trends of RR in the lower section

Figure 11
Flow velocity as a function of cumulative runoff for each section under the low (59 mm h^{-1}) and high (178 mm h^{-1}) rainfall intensities.

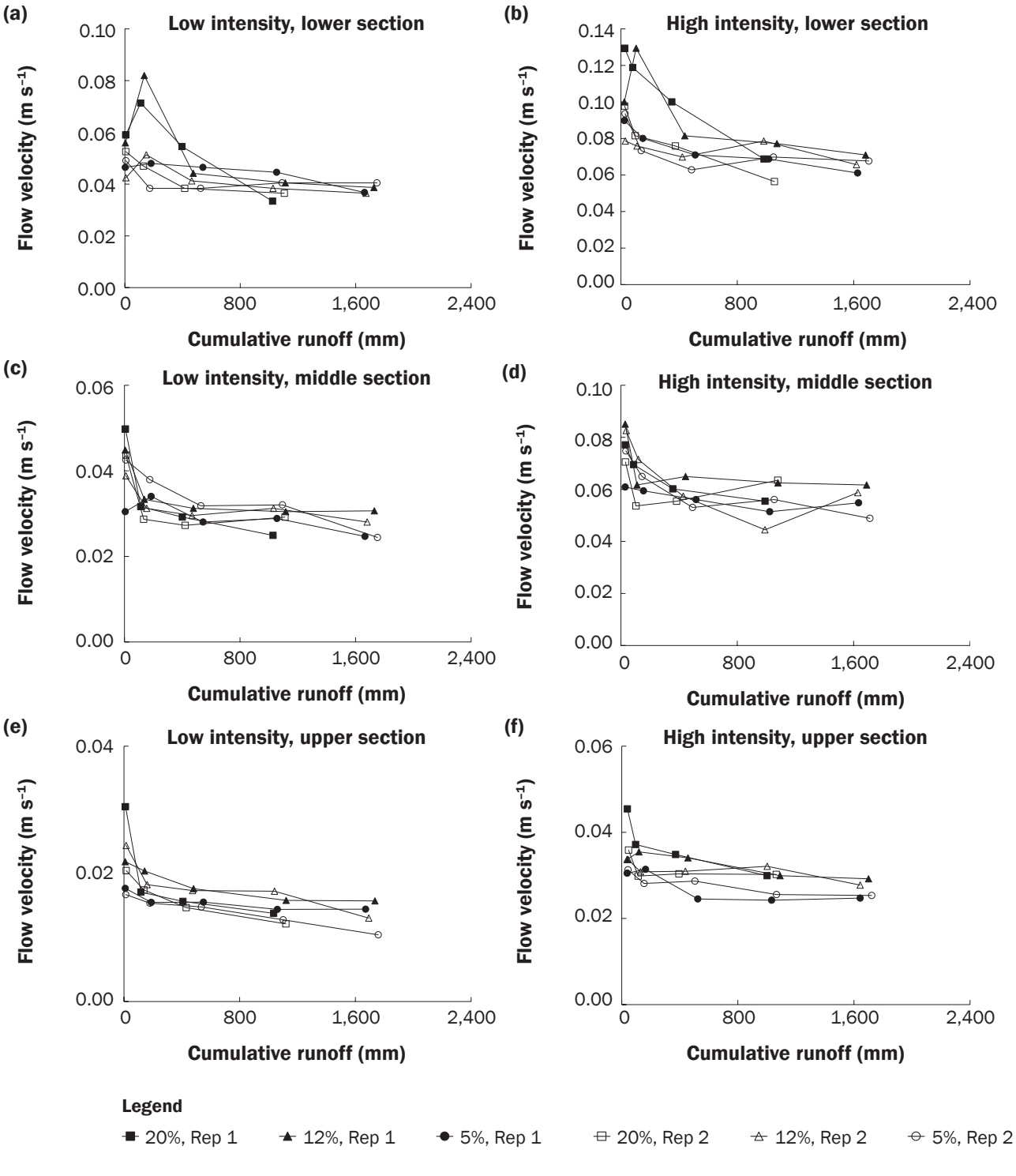

were contrary to the expectation of hydraulic roughness tracking rock cover changes. We used rock cover data in the lower section to examine the feasibility of utilizing the prediction model, which was derived from data in the middle and upper sections. The model performances were acceptable (figure 15) considering the complexity of flow patterns in the lower sections. These results emphasized the roles that surface rocks play in determining the overland flow velocity and hydraulic resistance, and also implied that

Figure 12
Terminal flow velocities from three sections under two rainfall intensities (59 mm h^{-1} and 178 mm h^{-1}) as a function of unit flow discharge (also reported by Nearing et al. [2017]).

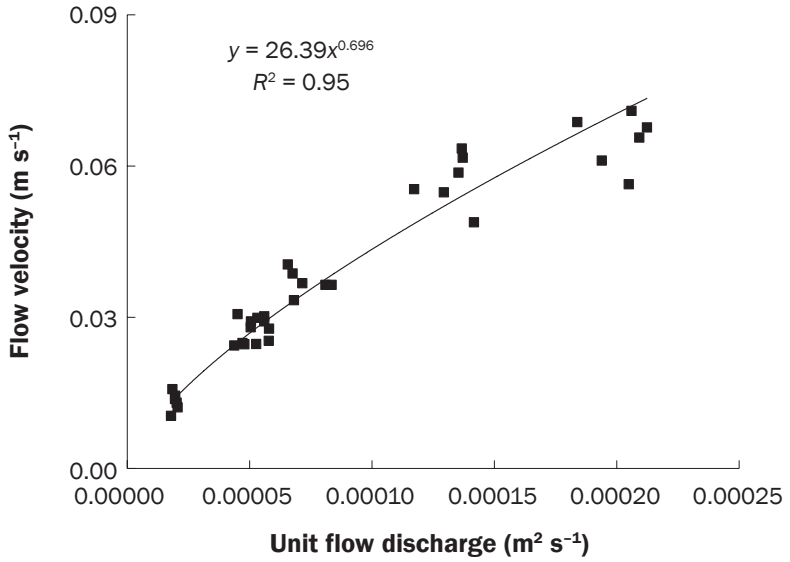

form resistance created by embedded or surficial rock was the dominant factor for these stony surfaces (Abrahams and Parsons 1991).

The Implications and Limitations of This Study. It is not easy to address the question of how hillslope roughness and rock cover evolve and interact with hydrologic processes over long-time periods using in situ field observations. Therefore, here we attempted to use rainfall simulation experiments to mimic the processes in which erosion pavement develops and to reveal the concomitant changes of surface morphology and overland flow velocity. Although our experiments are simplified models of natural hillslopes, they do suggest the existence of dynamic feedback mechanisms between the hillslope morphology and hydraulics, and suggest the direction in which hillslope would evolve under natural conditions. There is qualitative similarity between our results and

Figure 13
Flow velocity as a function of (a, b) average random roughness and (c, d) rock cover under (a, c) low rainfall intensity and (b, d) high rainfall intensity.

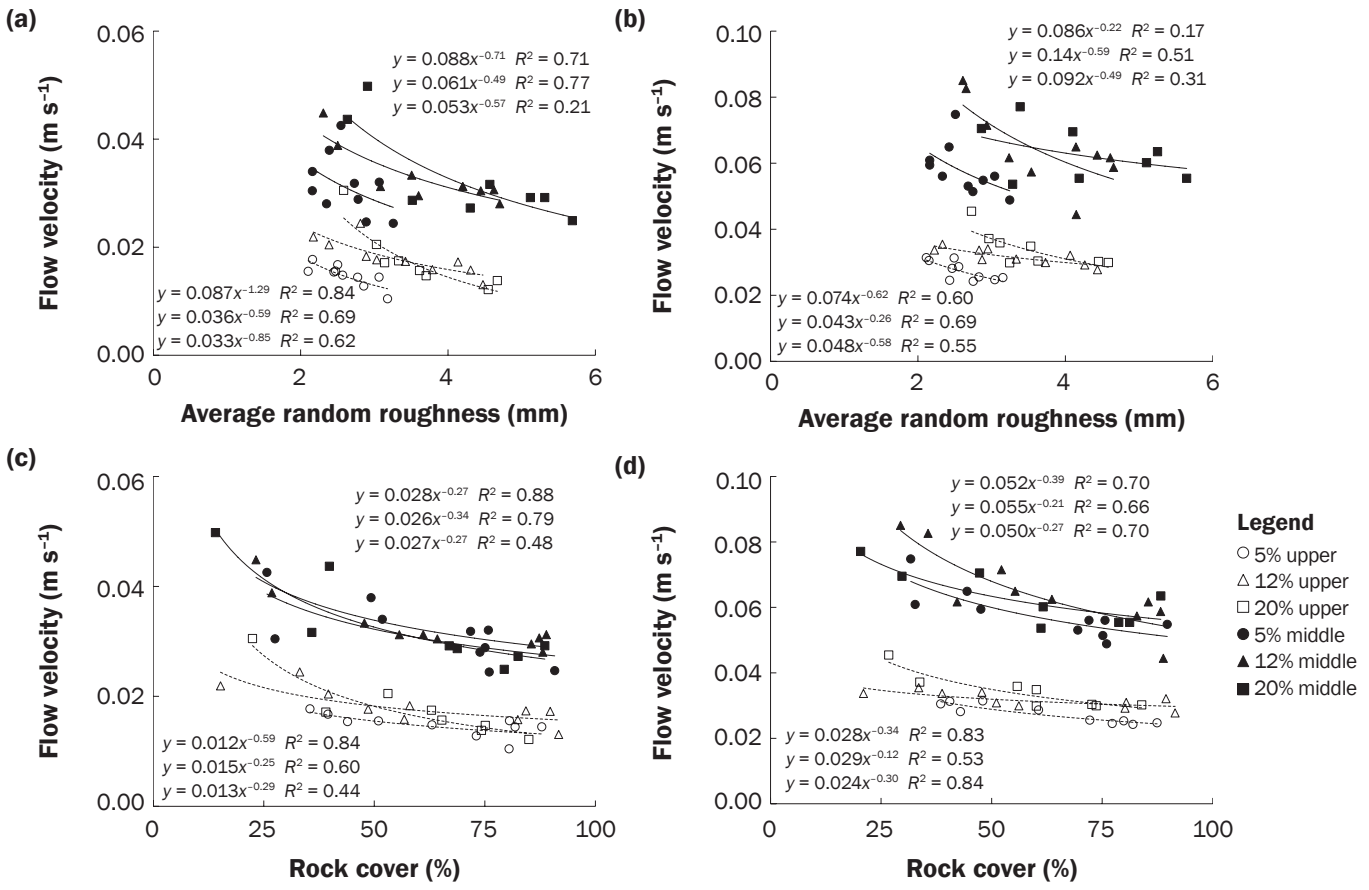

Figure 14
The hydraulic resistance [log(*f*)] as a function of (a, b) average random roughness and (c, d) rock cover under two rainfall intensities. (d) The Pearson correlation coefficients between hydraulic resistance predictor variables. (e) The prediction model of hydraulic resistance [log(*f*)].

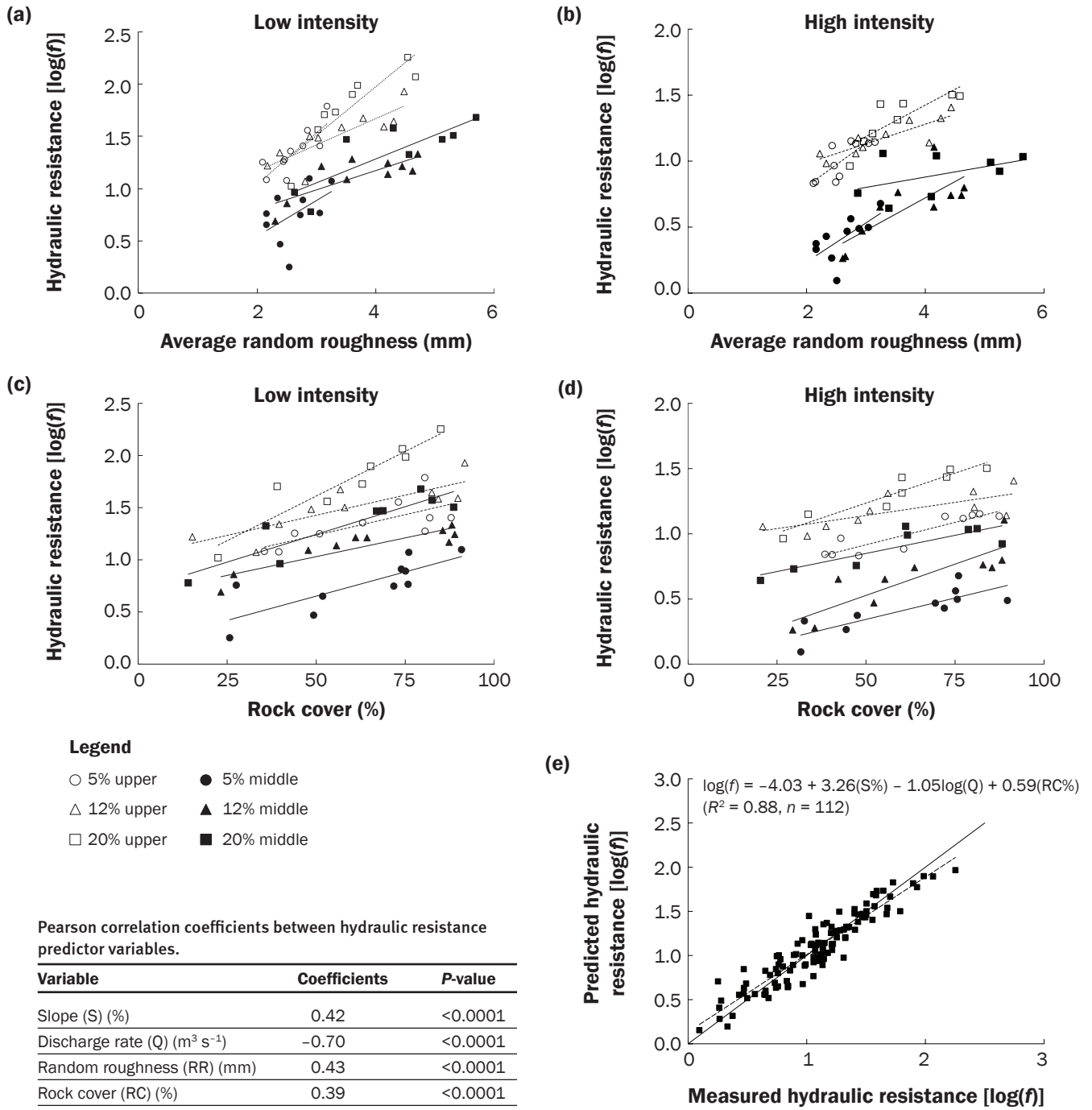

Pearson correlation coefficients between hydraulic resistance predictor variables.

Variable	Coefficients	*P*-value
Slope (S) (%)	0.42	<0.0001
Discharge rate (Q) ($m^3 s^{-1}$)	−0.70	<0.0001
Random roughness (RR) (mm)	0.43	<0.0001
Rock cover (RC) (%)	0.39	<0.0001

those evolutionary theories for large basins, for example the optimality principle. The basic idea of the optimality principle is that "the nature organizes itself in such a way that its functioning is optimal under given external forcing during steady state conditions" (Westhoff and Zehe 2013). One of many optimality principles is the Maximum Entropy Production, which relies on the fact that "a gradient drives a flux, while the same flux depletes the gradient" (Kleidon et al. 2013; Westhoff and Zehe 2013). This is seen in our study in that steeper slopes initially produced greater water flow velocity, while greater velocity induced greater morpho-

Figure 15
The predicted hydraulic resistances [log(*f*)] in the lower section using the model given in figure 14e and the discharge rate and rock cover data measured in the lower section.

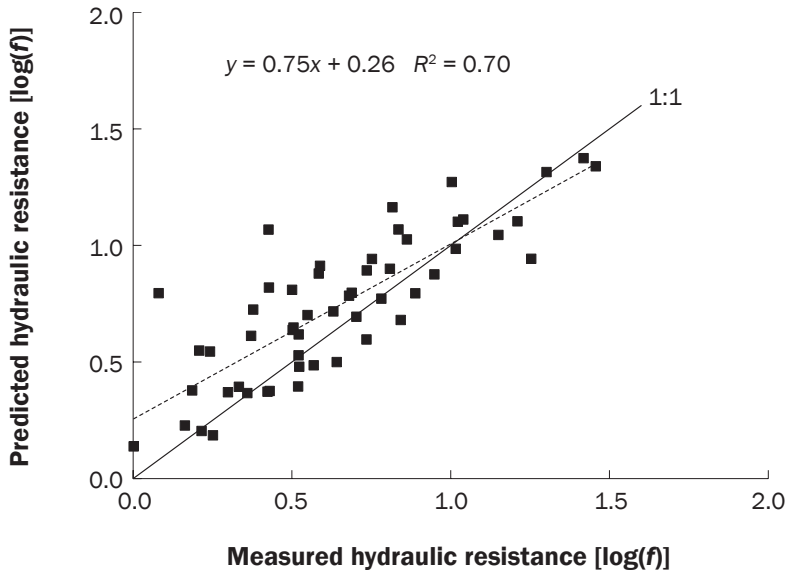

logical changes and hence greater hydraulic resistances, which counteracted the effects of the steeper slope gradient.

We used the surface characteristics (surface RR and rock covers) to predict the hydraulic friction and incorporate this relationship into statistical models. Our results indicated that hydraulic friction should also be related with the flow discharge rate and slope. Therefore, for a natural hillslope on which the rainfall-induced runoff rates vary with distance downslope and time during the rainfall events, the hydraulic frictions should be spatially and temporarily adjusted. One possible solution is to adjust the Manning coefficient based on the water depth (Rengers et al. 2016).

If the quantification of microtopography when rills were incised in the lower section of these plots is made without consideration of the area of surface inside and outside of the rills, misinterpretation of the data can be made, e.g., the apparent greater velocity with an accompanying decrease in the ARR. Addressing rill initiation and associated geometric changes over time is difficult to model. Al-Hamdan et al. (2013) developed an equation to use the unit flow discharge, slope, and ground cover to predict the probability of overland flow becoming concentrated on the plot scales. However, predicting the locations and numbers (or the spatial distributions) of those rills remains a challenge (Nouwakpo et al. 2016). With high-resolution mapping tools, such as LiDAR, delineating rills and dynamically recording their changes may be possible.

Summary and Conclusions

This study quantified the spatiotemporal evolution of rock cover and RR, and their effects on overland flow velocity as erosion pavement developed on 2 by 6.1 m plots. Rock cover increased as rainfall progressed because of the preferential removal of fine materials, but did not show slope dependence. The steeper slopes were associated with greater terminal surface roughness due to the combined effects of surficial exposed rock cover and erosion-induced microtopographic changes. The flow velocity predominantly decreased to reach a relative constant value for each section depending on the flow rates, which supported the theory of slope-velocity-equilibrium that flow velocity on an erodible, evolved surface will be a unique function of flow rates irrespective of slope gradient. Rock cover better explains the variabilities of flow velocities and hydraulic resistances than does surface RR. A model using flow discharge rate, slope gradient, and rock cover was given to predict the hydraulic resistance, suggesting that hydraulic friction was not predictable for a given surface condition but should also be related with slope gradients and flow rates. Our results also showed that the common perception that greater rock cover is always associated with greater surface roughness did not hold true for all cases.

Acknowledgements

We thank John Smith for the soil box preparation and soil collection. The Southwest Watershed Research Center hosted a number of workshops that helped in formulating the ideas in this manuscript. This study was funded by the USDA Agricultural Research Service.

References

Abrahams, A.D., and A.J. Parsons. 1991. Resistance to overland flow on desert pavement and its implications for sediment transport modeling. Water Resources Research 27:1827–1836, https://doi.org/10.1029/91WR01010.

Abrahams, A.D., and A.J. Parsons. 1994. Hydraulics of interrill overland flow on stone-covered desert surfaces. Catena 23:111–140, https://doi.org/10.1016/0341-8162(94)90057-4.

Abrahams, A.D., A.J. Parsons, and S.-H. Luk. 1986. Resistance to overland flow on desert hillslopes. Journal of Hydrology 88:343–363, https://doi.org/10.1016/0022-1694(86)90099-5.

Al-Hamdan, O.Z., F.B. Pierson, M.A. Nearing, C.J. Williams, J.J. Stone, P.R. Kormos, J. Boll, and M.A. Weltz. 2013. Risk assessment of erosion from concentrated flow on rangelands using overland flow distribution and shear stress partitioning. Transactions of the ASABE 56:539–548, https://doi.org/10.13031/2013.42684.

Bryant, R., M.S. Moran, D.P. Thoma, C.D. Holifield Collins, S. Skirvin, M. Rahman, K. Slocum, P. Starks, D. Bosch, and M.P. González Dugo. 2007. Measuring surface roughness height to parameterize radar backscatter models for retrieval of surface soil moisture. IEEE Geoscience and Remote Sensing Letters https://doi.org/10.1109/LGRS.2006.887146.

Bunte, K., and J. Poesen. 1993. Effects of rock fragment covers on erosion and transport of noncohesive sediment by shallow overland flow. Water Resources Research 29(5):1415-1424, https://doi.org/10.1029/92WR02706.

Ding, W., and C. Huang. 2017. Effects of soil surface roughness on interrill erosion processes and sediment particle size distribution. Geomorphology 295:801–810, https://doi.org/10.1016/j.geomorph.2017.08.033.

Gilley, J.E., E.R. Kottwitz, and G.A. Wieman. 1992. Darcy-Weisbach roughness coefficients for gravel and cobble surfaces. Journal of Irrigation and Drainage Engineering 118:104–112, https://doi.org/10.1061/(ASCE)0733-9437(1992)118:1(104).

Giménez, R., O. Planchon, N. Silvera, and G. Govers. 2004. Longitudinal velocity patterns and bed morphology interaction in a rill. Earth Surface Processes and Landforms 29:105–114, https://doi.org/10.1002/esp.1021.

Gómez, J.A., and M.A. Nearing. 2005. Runoff and sediment losses from rough and smooth soil surfaces in a

laboratory experiment. Catena 59:253–266, https://doi.org/10.1016/j.catena.2004.09.008.

Govers, G. 1992. Relationship between discharge, velocity and flow area for rills eroding loose, non-layered materials. Earth Surface Processes and Landforms 17(5):515-528, https://doi.org/10.1002/esp.3290170510.

Helming, K., M.J.M. Römkens, and S.N. Prasad. 1998. Surface roughness related processes of runoff and soil loss: A flume study. Soil Science Society of America Journal 62:243, https://doi.org/10.2136/sssaj1998.03615995006200010031x.

Holden, J., M.J. Kirkby, S.N. Lane, D.G. Milledge, C.J. Brookes, V. Holden, and A.T. McDonald. 2008. Overland flow velocity and roughness properties in peatlands. Water Resources Research 44, https://doi.org/10.1029/2007WR006052.

Huang, C., and J.M. Bradford. 1992. Applications of a laser scanner to quantify soil microtopography. Soil Science Society of America Journal 56:14, https://doi.org/10.2136/sssaj1992.03615995005600010002x.

Kleidon, A., E. Zehe, U. Ehret, and U. Scherer. 2013. Thermodynamics, maximum power, and the dynamics of preferential river flow structures at the continental scale. Hydrology and Earth System Sciences 17:225–251, https://doi.org/10.5194/hess-17-225-2013.

Li, G. 2009. Preliminary study of the interference of surface objects and rainfall in overland flow resistance. Catena 78:154–158, https://doi.org/10.1016/j.catena.2009.03.010.

Li. L, M.A. Nearing, M.H. Nichols, V.O. Polyakov, and M.L. Cavanaugh. 2019. Use terrestrial LiDAR to measure water erosion on stony plots. Accepted by Earth Surface Processes and Landforms.

Lv, J., H. Luo, and Y. Xie. 2019. Effects of rock fragment content, size and cover on soil erosion dynamics of spoil heaps through multiple rainfall events. Catena 172:179–189, https://doi.org/10.1016/j.catena.2018.08.024.

Moran, M.S., T.R. Clarke, W.P. Kustas, M. Weltz, and S.A. Amer. 1994. Evaluation of hydrologic parameters in a semiarid rangeland using remotely sensed spectral data. Water Resouces Research 30:1287–1297, https://doi.org/10.1029/93WR03066.

Nearing, M.A., A. Kimoto, M.H. Nichols, and J.C. Ritchie. 2005. Spatial patterns of soil erosion and deposition in two small, semiarid watersheds. Journal of Geophysical Research Earth Surface 110(F4), https://doi.org/10.1029/2005JF000290.

Nearing, M.A., V.O. Polyakov, M.H. Nichols, M. Hernandez, L. Li, Y. Zhao, and G. Armendariz. 2017. Slope-velocity equilibrium and evolution of surface roughness on a stony hillslope. Hydrology and Earth System Sciences 21:3221–3229, https://doi.org/10.5194/hess-21-3221-2017.

Nearing, M.A., J.R. Simanton, L.D. Norton, S.J. Bulygin, and J. Stone. 1999. Soil erosion by surface water flow on a stony, semiarid hillslope. Earth Surface Processes and Landforms 24:677–686.

Nouwakpo, S.K., C.J. Williams, O.Z. Al-Hamdan, M.A. Weltz, F. Pierson, and M. Nearing. 2016. A review of concentrated flow erosion processes on rangelands: Fundamental understanding and knowledge gaps. International Soil and Water Conservation Research 4:75–86, https://doi.org/10.1016/j.iswcr.2016.05.003.

Paige, G.B., J.J. Stone, J.R. Smith, and J.R. Kennedy. 2004. The Walnut Gulch rainfall simulator: A computer-controlled variable intensity rainfall simulator. Applied Engineering in Agriculture 20:25–31, https://doi.org/10.13031/2013.15691.

Parsons, A.J. 1991. Size characteristics of sediment in interrill overland flow on a semiarid hillslope. Earth Surface Processes and Landforms 16:143–152.

Parsons, A.J., A.D. Abrahams, and S.-H. Luk. 1990. Hydraulics of interrill overland flow on a semi-arid hillslope, southern Arizona. Journal of Hydrology 117:255–273, https://doi.org/10.1016/0022-1694(90)90096-G.

Parsons, A.J., A.D. Abrahams, and J. Wainwright. 1994. On determining resistance to interrill overland flow. Water Resources Research 30(12):3515–3521.

Pelletier, J.D. 2003. Drainage basin evolution in the Rainfall Erosion Facility: Dependence on initial conditions. Geomorphology 53:183–196, https://doi.org/10.1016/S0169-555X(02)00353-7.

Poesen, J., and H. Lavee. 1994. Rock fragments in top soils: Significance and processes. Catena 23(1-2):1-28, https://doi.org/10.1016/0341-8162(94)90050-7.

Poesen, J.W., D. Torri, and K. Bunte. 1994. Effects of rock fragments on soil erosion by water at different spatial scales: A review. Catena 23(1-2):141-166, https://doi.org/10.1016/0341-8162(94)90058-2.

Poesen, J.W., B. van Wesemael, K. Bunte, and A.S. Benet. 1998. Variation of rock fragment cover and size along semiarid hillslopes: A case-study from southeast Spain. Geomorphology 23:323–335, https://doi.org/10.1016/S0169-555X(98)00013-0.

Polyakov, V., and M. Nearing. 2019. A simple automated laser profile meter. Soil Science Society of America Journal 83:327, https://doi.org/10.2136/sssaj2018.10.0378.

Polyakov, V., M.A. Nearing, and J. Stone. 2018a. Velocities of shallow overland flow on semiarid hillslopes. Earth Surface Processes and Landforms 43:2578–2583, https://doi.org/10.1002/esp.4416.

Polyakov, V., J. Stone, C. Holifield Collins, M.A. Nearing, G. Paige, J. Buono, and R.L. Gomez-Pond. 2018b. Rainfall simulation experiments in the southwestern USA using the Walnut Gulch Rainfall Simulator. Earth System Science Data 10:19–26, https://doi.org/10.5194/essd-10-19-2018.

Rengers, F.K., L.A. McGuire, J.W. Kean, D.M. Staley, and D.E.J. Hobley. 2016. Model simulations of flood and debris flow timing in steep catchments after wildfire. Water Resources Research 52:6041–6061, https://doi.org/10.1002/2015WR018176.

Rieke-Zapp, D., J. Poesen, and M.A. Nearing. 2007. Effects of rock fragments incorporated in the soil matrix on concentrated flow hydraulics and erosion. Earth Surface Processes and Landforms 32:1063–1076, https://doi.org/10.1002/esp.1469.

Shaw, C.F. 1929. Erosion Pavement. Geographical Review 19:638-641, https://doi.org/10.2307/209694.

Simanton, J.R., K.G. Renard, C.M. Christiansen, and L.J. Lane. 1994. Spatial distribution of surface rock fragments along catenas in Semiarid Arizona and Nevada, USA. Catena 23:29–42, https://doi.org/10.1016/0341-8162(94)90051-5.

Simanton, J.R., and T.J. Toy. 1994. The relation between surface rock-fragment cover and semiarid hillslope profile morphology. Catena 23:213–225, https://doi.org/10.1016/0341-8162(94)90069-8.

Torri, D., and J. Poesen. 1992. The effect of soil surface slope on raindrop detachment. Catena 19:561–578, https://doi.org/10.1016/0341-8162(92)90053-E.

Torri, D., M. Sfalanga, and M. Del Sette. 1987. Splash detachment: Runoff depth and soil cohesion. Catena 14:149–155, https://doi.org/10.1016/S0341-8162(87)80013-9.

Van Wesemael, B., J. Poesen, T. De Figueiredo, and G. Govers. 1996. Surface roughness evolution of soils containing rock fragments. Earth Surface Processes and Landforms 21:399–411, https://doi.org/10.1002/(SICI)1096-9837(199605)21:5<399::AID-ESP567>3.0.CO;2-M.

Westhoff, M.C., and E. Zehe. 2013. Maximum entropy production: Can it be used to constrain conceptual hydrological models? Hydrology and Earth System Sciences 17:3141-3157, https://doi.org/10.5194/hessd-9-11551-2012.

Xia, L., X. Song, N. Fu, S. Cui, L. Li, H. Li, and Y. Li. 2018. Effects of rock fragment cover on hydrological processes under rainfall simulation in a semi-arid region of China. Hydrological Processes 32:792–804, https://doi.org/10.1002/hyp.11455.